



Mapping erosion-sensitive areas after wildfires using fieldwork, remote sensing, and geographic information systems techniques on a regional scale

F. Pérez-Cabello,¹ J. de la Riva Fernández,¹ R. Montorio Llovería,¹ and A. García-Martín¹

Received 30 November 2005; revised 16 March 2006; accepted 27 April 2006; published 8 September 2006.

[1] Alterations in the hydrological cycle following wildfire due to the loss of ground cover vegetation and changes in soil properties have been documented in many studies. Nevertheless, the rapid process of vegetation recovery reduces such negative effects. Vegetation cover before fire, fire severity, and geophysical properties are important factors that control spatial discontinuities involved in the vegetation-covering process. The objective of this study was to estimate the probability of high erosion in order to map erosion-sensitive areas after fire. The analysis was carried out in different plant communities burnt by summer wildfires in the pre-Pyrenean area (Spain). Three-year Landsat Thematic Mapper (TM) images have been used for mapping wildfire areas and severity levels. Conversion to spectral reflectance has been applied for radiometric correction by normalizing topographic and atmospheric effects. Likewise, other physical variables have also been incorporated into the geographic information system (GIS): vegetation types, parent material, illumination, slope, aspect, and precipitation. The dependent variable has been characterized by means of fieldwork and a photointerpretation process based on high-resolution digital aerial orthophotographs taken 11–12 years after the fire. Different logistic regression models have been used for mapping the probability of erosion. Results indicate that prefire normalized difference vegetation index values and aspect are the most important variables for estimating erosion-sensitive areas after fire (Nagelkerke $r^2 = 0.66$; Kappa values = 0.65). Finally, the use of nonparametric models with environmental digital information based on GIS can facilitate the management of burnt areas.

Citation: Pérez-Cabello, F., J. de la Riva Fernández, R. Montorio Llovería, and A. García-Martín (2006), Mapping erosion-sensitive areas after wildfires using fieldwork, remote sensing, and geographic information systems techniques on a regional scale, *J. Geophys. Res.*, *111*, G04S10, doi:10.1029/2005JG000148.

1. Introduction

[2] Wildfires are a natural disturbance in Mediterranean ecosystems. Long-standing forests in the Mediterranean Basin have been affected by fires for at least the last three million years [Naveh, 1974], defining a variety of forest compositions and structures, and shaping landscape properties [Trabaud, 2002]. Mediterranean-type ecosystems show great resilience to such disturbances [Keeley, 1986], with fire sometimes proving very important for forest conservation in providing advantages to fire-adapted vegetation communities. However, the negative effects from wildland fires (biomass loss, changes in successional patterns, alterations in soil properties, etc.) are today considered among the most important problems affecting forest degradation, since the natural capacity of Mediterranean plant communities to regenerate is being reduced. The

increase in the occurrence of large-scale and intense wildfires is principally due to the rapid changes in land use and climatic conditions (longer summer droughts, sudden storms, etc.) In fact, in the Mediterranean region approximately 50,000 fires affect 5000 km² of wooded land every year [Barbosa *et al.*, 2004] while in Spain around 150,000 ha of forest are burnt yearly.

[3] From a geomorphological point of view, wildfires alter the hydrological processes governing runoff infiltration generation and sediment production. Many studies have reported an increase in runoff and sediment yield rates after wildfires [Soto *et al.*, 1991; Soler and Sala, 1992; Dieckmann *et al.*, 1992; Helvey, 1980; Meyer and Wells, 1997; Robichaud and Brown, 1999; Cannon *et al.*, 2001; Meyer *et al.*, 2001; Moody and Martin, 2001; Cerdà and Doerr, 2005]. The destruction of ground cover vegetation and alterations in the physical and chemical properties of soil (water repellency and aggregate stability), due to the thermal impact of wildfires, are two of the most important factors impacting hydrological and geomorphological alterations. Vegetation cover consumption and litter duff alteration constitute the main factors affecting soil loss. A

¹Department of Geography and Spatial Management, University of Zaragoza, Zaragoza, Spain.

decrease in the amount of interception materials means that rain encounters fewer obstacles on its way toward the ground, leading to a major increase in its kinetic energy [Moody and Martin, 2001]. Consequently, its capacity to modify the soil aggregate stability is much greater [Mataix-Solera and Doerr, 2003], increasing soil erodibility. Although the dryness and ash-covered soil observed after fire may cause high infiltration rates [Cerdà, 1998], the main risk of erosion appears in the first few stages after the fire [Díaz-Fierros *et al.*, 1990]. In the medium term, erosion processes caused by forest fires depend on the interaction between ecological conditions, management practices [Naveh, 1974, 1990], and vegetation regrowth processes. Therefore a wide range of consequences may affect the relevant areas [Neary *et al.*, 1999], with nongeneralized tendencies readily apparent [Wondzell and King, 2003].

[4] Regarding postfire regeneration, many Mediterranean plant communities show effective regeneration mechanisms, such as resprouting from fire-resistant structures and/or seeding from fire-protected seeds. These mechanisms cause a rapid vegetation postfire recovery. In fact, such a rapid return to prefire conditions occasionally reduces the exposure time to erosion agents considerably [Trabaud, 1990; Vallejo and Alloza, 1998]. This recovery is designated the autosuccessional process [Hanes, 1971; Papió, 1988; May, 1991] and has been well documented. Several works describe this process, concluding that regeneration following a fire is similar to an autosuccessional process compensating a past regression [Naveh, 1990; Trabaud, 1990, 2002; Trabaud and Valina, 1998; Tárrega and Luis-Calabuig, 1987, 1989; Vera de la Fuente, 1994; Badía *et al.*, 1995]. However, specific sites may present difficulties for natural vegetation recovery, due to the unique interactions between fire impact and local factors, including topographic climatic influences, plant composition, topographic parameters, soil characteristics, land use history, or wildfire intensity. Thus methodologies capable of identifying those areas where erosion processes could be expected must be developed, in order to support vegetation and soil postfire restoration programs on a regional scale.

[5] There is widespread interest in mapping and predicting environmental processes, such as erosion, on a regional scale by means of predictive models [de Jong *et al.*, 1999]. To this end, the use of geographical information systems (GIS), digital elevation models (DEM), and multispectral remote sensing techniques offers interesting possibilities for developing such models. With respect to remote sensing imagery, satellite data and remote sensing techniques have been applied for the mapping of erosion [Bocco, 1991; Martínez-Casasnovas and Poch, 1998], and for collecting information regarding runoff and erosion models [de Jong *et al.*, 1999; King *et al.*, 2005]. Nevertheless, many of the parameters influencing infiltration and runoff (soil surface roughness, soil porosity, soil texture, and initial moisture content) are not directly accessible by satellite [King *et al.*, 2005].

[6] Concerning burnt areas, the impact caused by fire and the subsequent recovery process may be detected and monitored by means of remote sensing [Patterson and Yool, 1998; Bobbe *et al.*, 2001; Rogan and Franklin, 2001; Escuin *et al.*, 2002; Van Wagendonk *et al.*, 2004]. However, studies attempting to predict postfire erosion via integration

of this kind of data and techniques remain scant in the literature. In this respect, Ruiz-Gallardo *et al.* [2004] applied the normalized difference of the normalized difference vegetation index (NDVI) methodology to highlight postfire management requirements as they relate to the identification of potential erosion areas. Fernández *et al.* [2005] generated a susceptibility model for postfire soil erosion by means of mapping fire intensity. Other spatially distributed models for assessing fire impact on erosion and for identifying vulnerable areas prone to runoff increase are HEM-GIS [Wilson *et al.*, 2001] and SPLASH [Beeson *et al.*, 2001]. The former is an analytical hillslope erosion model integrated into a GIS framework while the latter simulates overland flow using Manning's equation on a landscape scale. Finally, in the USA, fire effects mapping has become standard practice for postfire resources management [Miller and Yool, 2002]. In fact, teams and researchers from the interagency burned area emergency rehabilitation (BAER) have developed different methodologies to minimize the effects of postfire erosion.

[7] Taking into account the variability of erosion after fire in the medium term, as well as the importance and advantages of remote sensing data and GIS technology for predicting these kinds of processes on a regional scale, the objective of the present study is to estimate the probability of high erosion after fire in order to better map erosion-sensitive areas. Different physical parameters (lithology, vegetation type, fire severity levels, slope, illumination, etc.) and spectral information (Thematic Mapper data) have been entered into a specific GIS while a nonparametric logistic regression (LR) model has been used to estimate the spatial distribution of probability. The results can assist forest managers not only in minimizing postfire erosion, but also in allocating resources for restoration efforts.

2. Site Description

[8] This study was conducted in different areas burnt in the years 1985 and 1986 (Table 1), located in a sector in the pre-Pyrenean range (1000 km²) in the north of Huesca province (Aragón, Spain) (Figure 1). This area has an extensive history of land use subjected to high levels of human pressure and is especially prone to wildland fires. The area has a very high geomorphological complexity with elevation ranging from 450 to 2000 m asl. The bedrock basically consists of limestone and sandstone, although there are also areas dominated by calcareous marl and superficial deposits associated with the fluvial network, restricted to the middle basin of the river Gállego. The spatial distribution of the different geomorphologic features and the diversity of the geologic units generate high topographic variations, with varied aspect and elevation values.

[9] The location of this area between continental Mediterranean (SE) and Atlantic influences (NE), in tandem with the topographic variations, generates a heterogeneous climate that can be generally defined as sub-Mediterranean with different levels of continental influence. The mean annual rainfall ranges from 750 to 1000 mm with an equinoctial rainfall pattern, with principal maximums occurring in spring and a slight water shortage in summer which is frequently interrupted by rainstorms. The mean annual

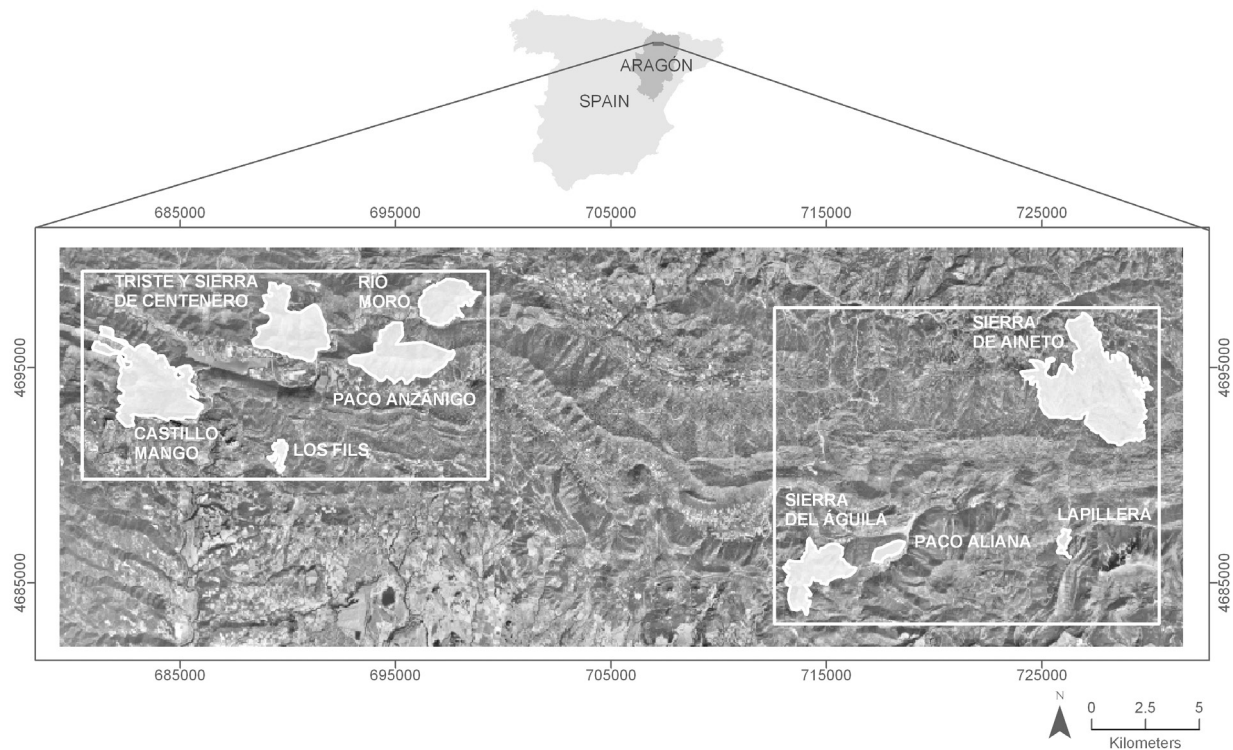


Figure 1. Orthophotography of the pre-Pyrenean region and location of the burnt areas examined in the study.

temperature ranges from 10°C to 12°C, with warm summers and a high risk of freezing in winter.

[10] Heterogeneity and a complex mixing of ecotypes and vegetation patches is the result of these geoclimatic variations. Geobotanic classification based on phytosociology association has identified four major classes: *Echinosparto horridi-Pineto Sylvestris sigmetum*, *Buxo sempervirentis-Querceto pubescentis sigmetum*, *Helleboro foetidi-Querceto rotundifoliae sigmetum*, *Violo willkommii-Querceto fagineae sigmetum* [Rivas-Martínez, 1987]. Moreover, plantation and reforestation of *Pinus sylvestris* and *Pinus nigra*, mixed with sub-Mediterranean shrub species (*Buxus sempervirens*, *Genista scorpius*, *Echinospartum horridum*), are also present. The great variation in lithological types, topographic position, aspect and vegetation types provides a large range of soil types. However, the most frequently

occurring are eutric and calcareous cambisols, regosols, leptosols, and calcisols.

3. Methods and Data

[11] The methodological approach to mapping erosion-sensitive areas after wildfire consists of successive phases, with the goal of obtaining all of the different variables included in the LR models, and then ultimately applying these models to estimate the dependent variable. Some of the techniques applied include remote sensing, GIS, fieldwork and statistical analysis. The abovementioned phases are detailed below. (1) Three Landsat images were selected and then preprocessing techniques applied to achieve a geometric and radiometric consistency. (2) Fire events that occurred in the study area during 1985–1986 were mapped

Table 1. Wildfires and Burnt Areas Analyzed During the Period 1985–1986

Fire Name	Fire Date		Burnt Area, ha		
	Ignition	Extinction	Total	Tree Area	Nontree Area
Los Fils	26 July 1985	28 July 1985	100	100	0
Solano de Triste	5 August 1985	12 August 1985	700	600	100
Paco Anzánigo	23 August 1985	28 August 1985	1050	40	1010
Paco Aliana	15 September 1985	16 September 1985	1980	0	1980
Barranco del Río Moro	31 July 1986	3 August 1986	550	21985	265
Umbría de la Srra. de Aineto	31 July 1986	8 August 1986	2270	2150	120
Sierra del Águila	6 August 1986	10 August 1986	19800	125	675
Lapillera	23 August 1986	25 August 1986	1980	1980	0
Castillo Mango	25 August 1986	27 August 1986	900	200	700

using RGB (743) false color band combinations and prefire and postfire NDVI values. (3) Burn severity was mapped using the differenced normalized burn ratio (ΔNBR) with an extended perspective. (4) GIS was used to map geophysical features. (5) An erosion database was obtained from ground-based measurements and photointerpretation analysis. (6) The LR was then applied.

3.1. Selection Images and Preprocessing

[12] Three Landsat 5 Thematic Mapper (TM) images (path 30, row 199), recorded in August 1984 (prefire), September 1986 and July 1987 (postfire) were acquired. They were selected based on the temporal coincidence of the large wildfires that occurred during the dry seasons in 1985 and 1986 and the degree of cloud cover. Thus the 1984 image captures prefire spectral features from the burnt areas while the 1986–1987 images capture postfire spectral features from areas burnt in 1985 and 1986, respectively. As can be inferred from the dates of these images, all of the analysis applied in the burnt areas were conducted based on a medium-term perspective by waiting until the following year.

[13] Because of the importance of correctly comparing these images, two considerations were taken into account. (1) To minimize problems associated with the different vegetation phenology, all of the images analyzed correspond to the same season. As in the study area there is an important presence of deciduous communities, thus it was necessary to select summer for correctly analyzing fire severity and green biomass recovery (e.g., foliage shedding of *Q. gr. cerrioides* in October–November could had been assessed as a lack of regeneration, instead of a loss of green biomass stemming from phenology). (2) An analysis of rainfall collected during 1984, 1986, and 1987 was carried out to assess its potential influence on the green biomass present in the collected images. The annual rainfall in 1984 was 59 mm higher than in 1986, and 41 mm higher than in 1987 (Table 2). Nevertheless, if the analysis is constrained to the rainfall with influence on fuel moisture content during the dry season, that collected from May vis-à-vis each image date, the differences are much less pronounced: only 7 mm between 1984 and 1986, and 2 mm between 1984 and 1987.

[14] Prior to conducting our analysis, all of the images were geometrically corrected. The importance of an accurate geometric rectification in this research is evident due to the fact that three Landsat images were used and the image data were linked with information derived from a digital elevation model (DEM). Accordingly, a subset of the 1986 image framing all of the study area was geometrically rectified into a local UTM projection (International 1909 Ellipsoid, European Datum 1950, Zone 30 North) using a second-order polynomial model included in ERDAS

IMAGINE 8.7. In this rectification model, we incorporated the DEM acquired from the Instituto Nacional de Información Geográfica (CNIG) of Spain (pixel size = 10×10 m). Ground control points (GCPs) were taken from high spatial resolution orthophotographs available in digital format (pixel size = 1×1 m). Our aim was to correlate the image to the referenced UTM projection with an estimated error lower than 1 pixel (30 m). A total of 104 GCPs was used to reproject the data with an estimated RMSE of 0.50 pixels. A nearest-neighbor resampling technique was used to minimize changes in the radiometric values of the ground data, with the pixel reprojected to 25 m. Moreover, the 1986 image was used as a reference to coregister the 1984 and 1987 images.

[15] Likewise, to compensate for variations in the sensor radiometric response, as well as for the natural conditions of solar radiance and solar angles, we converted our data to spectral reflectance values by normalizing the topographic and atmospheric effects. First, a revision of the dark object method [Chavez, 1996] was applied to eliminate the atmospheric effects present in all-optical remote sensing images. Second, conversion from digital values to reflectance was carried out by means of a method proposed by Pons and Solé-Sugrañes [1994]. Accordingly, reflectance was computed as follows:

$$\rho_k = (K\pi(L_{sen,k} - L_{a,k})) / (E_{0,k}(\cos\theta_i)^2) \quad (1)$$

$$K = (1 + 0.0167(\text{sen}(2\pi(D - 93.5)/365))) \quad (2)$$

where ρ_k is the reflectance for band k , K is a factor that takes into account the variation of the Sun-Earth distance (computed as a function of the Julian day D), $L_{sen,k}$ is the radiance detected by the sensor (computed from the digital values using the calibration coefficients included in the image), $L_{a,k}$ is the atmospheric radiance (computed from the minimum dark object value of the band), $\cos\theta_i$ is the cosine of the incidence angle, and $E_{0,k}$ is the solar irradiance at the top of the atmosphere and the solar zenith angle.

3.2. Mapping Burnt Areas

[16] Since changes in radiometric response are produced after fire due both to the sudden decrease in plant recovery and to changes in soil properties [Jakubauskas et al., 1990; Díaz-Delgado et al., 2003], including the increase of soil exposure, satellite images are an efficient way to map burnt areas [Minnich, 1983], to analyze damage levels [Siegert and Hoffmann, 2000], and to monitor plant response on a regional scale [Díaz-Delgado and Pons, 2001].

[17] Many methods for discriminating the radiometric effects caused by wildfires have been developed. Principal components analysis [Fung and LeDrew, 1987; Conese et al., 1988], Kauth-Thomas transformation [Collins and Woodcock, 1996; Crist and Cicone, 1984], and spectral vegetation indices [Townshend and Justice, 1986; Kasischke and French, 1995] are some of the most commonly employed techniques. In the latter method, the NDVI [Tucker et al., 1985] has been the most frequently used for monitoring, analyzing, and mapping temporal and spatial postfire variations, as it integrates two of the most important bands for vegetation discrimination. These bands, combined

Table 2. Rainfall Data of the Periods Between the Available Images

Image Date	Annual Rainfall, mm	Rainfall Average From May to Available Image Date, mm
1984	780	56 (May, July, August)
1986	721	49 (May, July, August, September)
1987	739	54 (May, July)

as shown in the equation below, constitute the near-infrared (NIR), from 0.76 to 0.90 μm , which is particularly responsible for the amount of vegetal biomass, and the visible red reflectance (R), from 0.63 μm to 0.69 μm , which is useful for soil boundary.

$$\text{NDVI} = (\text{NIR} - \text{R}) / (\text{NIR} + \text{R}) \quad (3)$$

The burnt area perimeter was delimited using a RGB (743) false color band combination of the 1986 image and the difference between the NDVI prefire and postfire [Pérez-Cabello and de la Riva, 1998; Viedma et al., 1997]. The RGB image shows a strong contrast between the pink and red colors, which correspond to the burnt area, and the green and brown colors associated with the living or slightly burnt vegetation (Figure 2). With regard to the NDVI values, the average value in the burnt areas one year after the fire was approximately 0.44 while the average prefire NDVI was about 0.63 (Figure 3a). However, differences based on vegetation type and the burnt area are evident; e.g., while a burnt plot of *Quercus gr. cerrioides* woodland shows a mean value of 0.45, a *Pinus sylvestris* woodland tract shows a mean value of 0.37. On the other hand, small differences have been observed among NDVI values based on the three images; e.g., in a nonburnt control plot (170 hectares) differences <0.023 have been detected. This fact ensures the comparability of the analysis for the areas burnt in two different years.

3.3. Mapping Burn Severity

[18] Regarding damage level, fire severity can be understood as a measure of the effects of fire on ecosystem components [Key and Benson, 2006]. Moreover, fire severity is very important for understanding fire effects on both postfire vegetation succession [Epting et al., 2005] and postfire hydrological processes. Generally speaking, high-severity burnt areas register higher rates of soil loss [McNabb and Swanson, 1990] and lower rates of vegetation

recovery, due to the higher consumption of the forest floor and canopy [Robichaud and Waldrop, 1994; DeBano et al., 1998]. Therefore the impact is more permanent over time.

[19] To map burn severity, the normalized burnt ratio (NBR) was calculated [Key and Benson, 2006]. This index integrates the two most responsive bands, albeit in opposite ways, to burning: NIR (from 0.76 to 0.90 μm) and mid-infrared (SWIR) (from 2.08 to 2.35 μm) combined as shown in the equation below.

$$\text{NBR} = (\text{NIR} - \text{SWIR}) / (\text{NIR} + \text{SWIR}) \quad (4)$$

To provide a quantitative measure of change, the ΔNBR is obtained by subtracting the NBR data set derived after burning from the NBR data set derived from before burning.

$$\Delta\text{NBR} = \text{NBR}_{\text{prefire}} - \text{NBR}_{\text{postfire}} \quad (5)$$

[20] Two strategies for processing and applying ΔNBR are possible [Key and Benson, 2006]. The first strategy, the initial assessment, refers to the most immediate fire effects to those biophysical components that existed before the fire. It uses a postfire Landsat TM/ETM+ image from as soon after the fire as possible and a prefire image of a similar period from the previous year. The second strategy, the extended assessment, uses a postfire Landsat TM/ETM+ image from a year after the fire and a prefire image from a year or two before the fire, so long as the area conditions are comparable. By waiting until the following growing season, the vegetation has time to recover. This approach is ideal for studies that compare several fire-affected areas over time. It is also better for studying ecological processes, such as erosion. For these reasons, this extended approach was the one selected for our own research.

[21] The ΔNBR image is hypothesized to correlate with the environmental changes caused by a fire. Accordingly, Key and Benson [2006] indicated that the NBR strongly

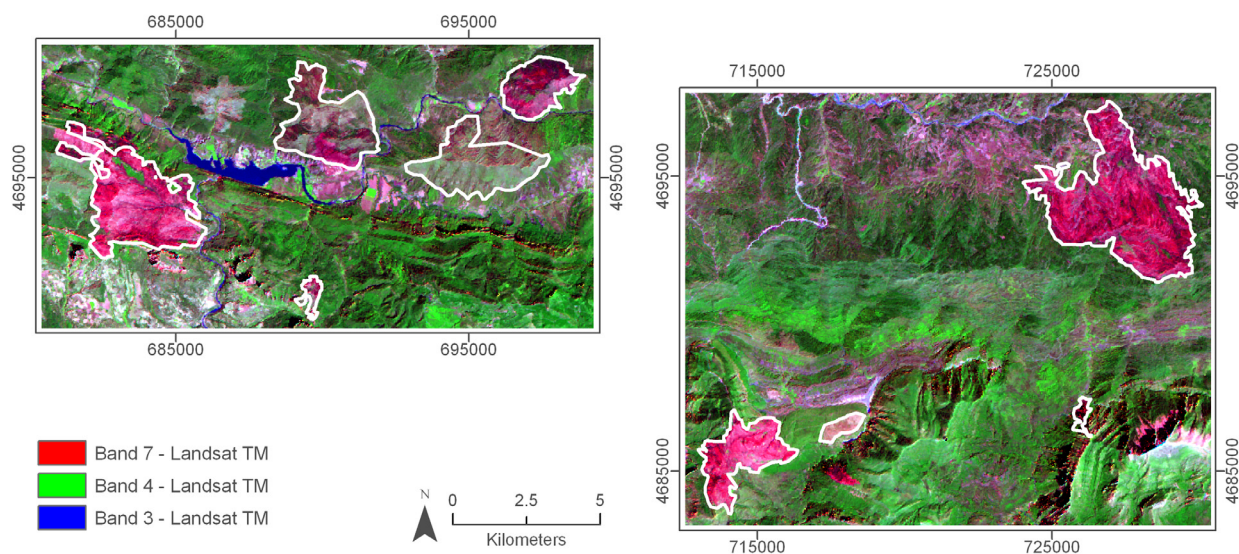


Figure 2. False color band combination 7/4/3 (RGB) of the study area in 1986. Fire perimeters are shown in white.

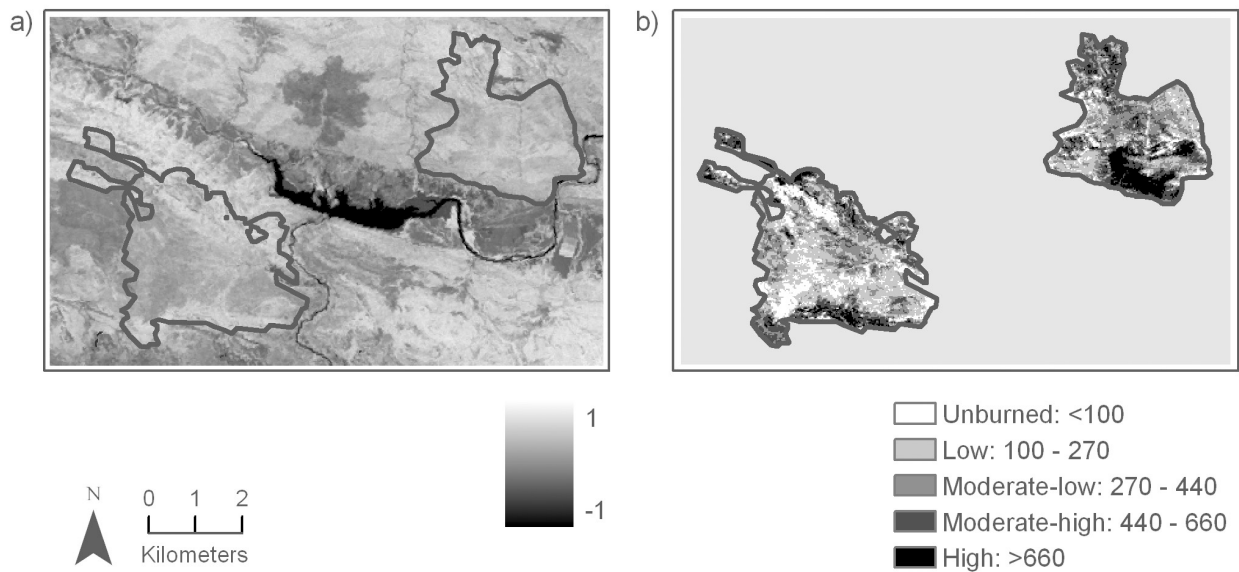


Figure 3. Spatial distribution of spectral features selected by the models. These variables are shown only in the two selected fires, Triste-Sierra de Centenero and Castillo Mango, corresponding to those areas burnt in 1985 and 1986, respectively. (a) Spatial distribution of the NDVI in pre-fire conditions (1984). (b) Spatial distribution of severity levels. In the areas burnt in 1985, the ΔNBR was computed as the difference between the prefire NBR (1984) and the postfire NBR (1986). In the areas burnt in 1986, the ΔNBR was computed as the difference between the prefire NBR (1984) and the postfire NBR (1987). In both cases, an extended perspective was applied by using an image from the year following the fire; moreover, the continuous image was categorized into severity levels according to the FIREMON methodology.

correlates with the composite burn index (CBI); nevertheless, this index may not be appropriate for estimating burn severity in nonforested areas [Epting *et al.*, 2005].

[22] The continuous ΔNBR data set can be stratified into ordinal classes, or severity levels (Figure 3b). According to the FIREMON methodology, four severity levels can be observed inside the burnt areas, based on a combination of different factors such as aspect, slope, weather conditions, and particularly vegetation structure and floristic composition. The spatial distribution of these severity levels in the burnt areas surveyed in the present study shows that the highest levels occurred on north facing slopes, where tree plant communities (*Pinus sylvestris* and *Pinus nigra*) occupied large areas, while the lowest levels occurred on south facing slopes which were occupied by nontree plant communities.

3.4. Geophysical Features

[23] In addition to the predictors extracted from satellite images (reflectance values from prefire images and ΔNBR), other types of geophysical variables such as vegetation types, vegetation structure, floristic composition, lithology, illumination, slope, aspect, and climatic variables were incorporated into a specific GIS in order to evaluate the control exerted by these variables on postfire erosion.

[24] Vegetation communities affected were identified by means of a multispectral supervised maximum likelihood classification (Euclidean distance normalized by variance) applied to the 1984 Landsat TM image using the six non-thermal bands. Training sites were selected based on both field knowledge and the Forest Map of Aragón (1:50,000)

[Ruiz de la Torre, 1992]. The final classification accuracy obtained was 78.55% (overall Kappa statistics = 0.74). The algorithm enabled us to specify different facies of *Pinus sylvestris*, *Pinus nigra*, *Pinus halepensis*, *Quercus rotundifoliae* and *Quercus* group *cerrioides*, as well as shrublands of *Buxus sempervirens*, *Echinopartum horridum* and *Genista scorpius*. These plant communities were categorized into two types, according to the dominant species and their regenerative traits: seedling species and sprouting species. Structural parameters were also categorized into two groups: tree plant communities and shrub plant communities.

[25] Lithology was obtained from the Geological Map of Spain, distinguished into two categories, soft rocks (silts and clays) and hard rocks (limestone and sandstones). Figure 4a shows the spatial distribution of the different lithological types. Topographic data are a prerequisite to any hydrologic or geomorphologic study [King *et al.*, 2005]. In this case, slope angle, aspect, and illumination data were obtained from the digital elevation model available and calculated using the routines found in ERDAS IMAGINE version 8.7. Subsequently, aspect was classified into two groups: NW, N and NE exposures in the first and E, W, SE, SW and S exposures in the second. Figures 4b and 4c represent the spatial distribution of illumination and aspect.

[26] Finally, climatic variables (mean annual temperature and precipitation) and climatic indices (Thermicity and Fournier) mapping was carried out using multiple-regression models. These models are based on the relationships between geotopographic variables derived from the DEM and climatic data. The predictors used were as follows: x

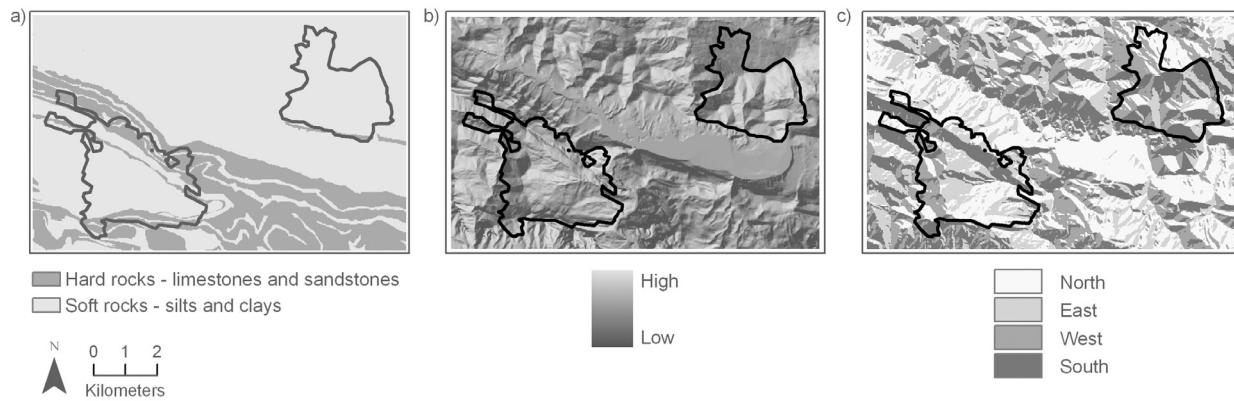


Figure 4. Spatial distribution of the geophysical features selected by the models. These variables are shown in the same two fires selected previously. (a) Lithological map classified as a function of rock hardness. (b) Illumination map obtained using solar angles corresponding to the prefire image (1984). (c) Aspect map obtained from the DEM.

coordinate (latitude), y coordinate (longitude), and z coordinate (elevation) while climate data recorded from 24 thermopluviometer stations over a period of 23 years (1973 to 1995) was the dependent variable. Further details can be found in the work of Pérez-Cabello [2002]. The Fournier index is used to determine the influence of rainfall on the erosion processes. This index is calculated as the division between the square of the amount of rainfall during the wettest month and the annual precipitation (mm). On the other hand, the Thermicity index is one of the bioclimatic indices included in the Rivas-Martinez methodology [Rivas-Martínez and Loidi, 1999] for establishing a generic worldwide climate classification. It is calculated as 10 times the sum of the yearly average temperature (T), the average minimum temperature of the coldest month of the year (m) and the average maximum temperature of the coldest month of the year (M). In this case, it was used as a tool to characterize the influence of climate on postfire vegetation processes.

3.5. Obtaining an Erosion Database

[27] Obtaining the dependent variable is based on knowledge of the intensity and spatial distribution of erosion processes in burnt areas. Two steps had to be completed to obtain this variable: (1) fieldwork, to evaluate erosion by measuring different biological, pedological, and geomorphological indicators; (2) photointerpretation of erosion and vegetation recovery areas from high spatial resolution orthophotographs. The first stage, surveying field plots, is the most reliable source of reference data for determining erosion level distribution. However, if the number of the plots is not sufficient to conduct a statistical analysis, aerial photographs can be used to assess the erosion level distribution, thereby enhancing database size. Both methodologies are presented below.

3.5.1. Data Set Based on Fieldwork

[28] Fieldwork was carried out during the summer of 1999. A total of 46 plots, of 100 m², was surveyed inside the burnt areas, grouping the different vegetation communities affected by the fires that occurred in 1985 and 1986. Areas affected by logging, afforestation, or pasturing were eliminated. For each plot, three types of indicators were quantified to evaluate the

magnitude of erosion: (1) those related to erosion levels, (2) those related to soil erodibility levels, and (3) those related to the vegetation regeneration processes.

[29] To recognize erosion levels, a group of phenomena was selected assessing by visual inspection their superficial incidence. Visual criteria were used to identify the hydrological erosion processes described in the Food and Agricultural Organization (FAO) provisional methodology for the evaluation of soil degradation [FAO, 1980]. The spatial incidence, in terms of percentage, of the following erosive manifestations was collected: accumulations of fine material over roots and branches; the presence of exposed roots and scars; the formation of erosion pavements, erosion pedestals and drainage incisions in the flow lines (rills and gullies). To determine the pedologic parameters, we followed those categories listed in the guide for soil profile descriptions [FAO, 1977], extracting the following indicators: depth of the organic horizons (A_{00} and A_0); structure and texture of A horizon; consistency, size and shape of the aggregates of A horizon; pH, carbonates and organic matter content. In evaluating the level of vegetation cover, i.e., the perpendicular projection of each stratum's aerial parts, was collected following the Braun-Blanquet [1979] methodology, and incorporating the stratum analysis of Bertrand [1966]. Subsequently, the 46 samples were grouped into two categories: high (1) and low (0) erosive activity, with 15% of the active surface used as the threshold for distinguishing between the two groups. Tables 3, 4, and 5 show the average values of the indicators used for the two types of dependent variable. In general terms, a higher soil degradation level was observed in group 1. Moreover, changes in postfire erosion seem to have been related to vegetation recovery. Regarding the

Table 3. Average Values of Erosion^a

	Plots	Bare Soil, %	a	b	c	d	e	f
(0)	21	11.6	0.3	0.3	1.7	2.7	0.0	0.7
(1)	25	30.2	2.3	1.7	4.3	11.0	0.3	4.6

^aHere 0 indicates plots with low erosion; 1 indicates plots with high erosion. Erosive manifestations measured in percentage levels are as follows: a, accumulations of fine material over roots and branches; b, presence of exposed roots; c, scars; d, formation of erosion pavements; e, erosion pedestals; f, drainage incisions in the flow lines (rills and gullies).

Table 4. Pedological Features Used to Assess Erosion^a

	Plots	Depth Organic Layer, cm	Organic Matter	Aggregate Consistency	Aggregate Size	Aggregate Shape	Carbonates
(0)	21	0.9	9.1	slightly hard	thin-medium	subangular-angular	9.2
(1)	25	0.6	8.8	Soft	thin-very thin	subangular-granular	13.1

^aHere 0 indicates plots with low erosion; 1 indicates plots with high erosion.

latter, a statistically significant correlation at the 0.01 level (two tailed) between erosion and postfire vegetation recovery (Pearson correlation = -0.622) was observed. Significant differences in the recovery processes vis-à-vis erosion groups (1 and 0) were also observed.

3.5.2. Data Set Based on Photointerpretation Analysis

[30] Taking into account results from fieldwork, as well as the usefulness of photointerpretation techniques, a second method to enhance the calibration data set was employed. The data set based on fieldwork was overlaid onto digital orthophotographs, with chromatic and textural keys correlating to erosion levels then identified from them. According to these keys, and based on the relationships between vegetation recovery and postfire erosion, 160 polygons of variable size were digitalized, always next to the fieldwork plots. An erosion level (1 or 0) was then assigned to the new polygons according to the criterion of minimum distance. ESRI's ArcGIS was utilized for this phase.

3.6. Application of the Logistic Regression

[31] A LR model, a special case of multiple regressions, has been successfully applied in numerous studies: mapping landslide susceptibility [Gorsevski *et al.*, 2000; Ohlmacher and Davis, 2003], human fire risk [Chuvienco *et al.*, 2004], spatial distribution of vegetation species [Aspinall, 2002], or the identification of large-scale interannual forest cover changes [Fraser *et al.*, 2005]. These studies have demonstrated good results for estimating the explanatory capacity of such predictor variables.

[32] In this study, LR was used for mapping the probability of high erosion in the burnt areas of pre-Pyreanean. The principle underlying LR is that a phenomenon measured with a dichotomous variable is determined from independent predictors [Menard, 1995]. There is nonrestriction on the independent variables, except that they cannot be linearly related. In this case, the goal of the LR model was to describe the relationship between a set of independent variables and two levels of erosion: (1) high erosion and (0) low erosion. Three kinds of trials were carried out to find the best fitting model and to rank the relative importance of the independent variables. The Maximum likelihood estimation was the method used to calculate the logistic coefficients (the natural logs of odds ratios), with a stepwise LR procedure then applied. This model fits the dependent variable using the equation below:

$$P(y = 1/X) = \exp\left(\sum BiXi\right) / 1 + \exp\left(\sum BiXi\right) \quad (6)$$

where P is the probability of the dependent variable, and Xi and Bi are the independent variables and the estimated coefficients of the model, respectively.

[33] The relative importance of the variables included can be assessed using the corresponding β and $\exp(\beta)$ coefficients in each model. The former indicates the estimated coefficient in the model while the latter, the antilogarithm transformation of β , refers to the predicted change in odds for each unit of increase in the predictor. The odds ratio is the relationship between the probability of being true and the probability of not being true. When β is positive, $\exp(\beta)$ will be greater than 1 and the odds ratio will increase; when β is negative, the antilogarithm will be lower than 1, and the odds ratio will decrease. The global measure of model fitting has been evaluated by the likelihood value $-2LL$, the Hosmer and Lemeshow test, and the Nagelkerke r^2 .

[34] The significance of the predictors was assessed by means of the Wald test. Prior to applying the LR models, two previous analyses were carried out. The first removed from the analysis pixels of bare soil or scarcely covered areas by defining the prefire NDVI value of 0.2 as the threshold for pixel inclusion in the model. The second analyzed, by means of Pearson coefficients, the correlation between covariables in order to not break the only requisite of the LR models. Thereafter, two groups of variables were considered: spectral and geophysical.

[35] To validate the final result, only 80% of the sample was selected as a calibration data set ($n = 636$) while the remaining 20% was used to test the model. Concerning the calibration data set, 337 pixels had a value of 0 (low erosion) while 299 pixels had a value of 1 (high erosion). A confusion matrix, as well as overall Kappa statistics [Congalton and Green, 1999], was generated to assess the models' accuracy. The statistical analysis was developed using SPSS v.12. To generate the final probability map, image processing and data compilation were carried out using ERDAS IMAGINE version 8.7.

4. Results

[36] After having applied the Pearson correlation analysis to the continuous variables, we selected those to be introduced into the different LR models which are shown in Table 6. The ΔNBR and TM bands 3 and 4 were included as spectral continuous variables. Elevation, slope, illumination, and Fournier were included as geophysical continuous variables while aspect, lithology, and vegetation (structure and regeneration strategy) were included as dummy varia-

Table 5. Vegetation Parameters Used to Assess Erosion Measured in Percentage Levels^a

	Plots	Stratum 1	Stratum 2	Stratum 3	Stratum 4	Stratum 5	Accumulated Recovery
(0)	21	74.4	29.2	26.4	6.9	0.8	136.3
(1)	25	50.0	29.0	31.1	3.7	0.0	116.0

^aHere 0 indicates plots with low erosion; 1 indicates plots with high erosion.

Table 6. Independent Variables Introduced in the First LR Model

Name	Type
ΔNBR	continuous
TM band 3	continuous
TM band 4	continuous
Elevation	continuous
Slope	continuous
Illumination	continuous
Fournier index	continuous
Vegetation: structure	categorical
Vegetation: regeneration strategy	categorical
Lithology	categorical
Aspect	categorical

bles. Precipitation, Thermicity index, and TM bands 1, 2, 5, and 7 were excluded from the LR modeling due to the high autocorrelation among them (Pearson coefficient > 0.4).

[37] With these selected variables, the first LR model (model 1) was constructed; its overall statistics are summarized in Table 7. Nagelkerke r^2 indicates a good correlation between the selected variables and the erosion categories. More than 60% of the variations surrounding the dependent variable are explained by this model (Nagelkerke $r^2 = 0.65$). The Hosmer-Lemeshow test indicates that the model adequately accommodates the data (p value = 0.117), while the overall Kappa statistic, which evaluates the model's accuracy, indicated that a fair percentage of the data was correctly classified (0.60). ΔNBR, TM bands 4 and 3 from the prefire image (1984), illumination, as well as the dummy variables lithology and aspect are the most important factors in determining the probability of high erosion. On the other hand, slope, elevation, Fournier index values, and vegetation parameters such as structure and regeneration strategy were not selected by this model. Regarding the relative importance of the selected variables, all of the coefficients, except those corresponding to TM band 4 and the dummy variable lithology, show positive signs and $\exp(\beta)$ values greater than 1. Therefore ΔNBR, illumination, TM band 3, and areas predominantly occupied by soft lithologies positively correlate with the probability of high erosion. Likewise, $\exp(\beta)$ coefficients of illumination, ΔNBR, and TM bands indicate that they only slightly impact the dependent variable while aspect and lithology are the best estimators in this model (Table 8).

[38] Given the sign and the levels of participation for the different spectral variables in the first model (β coefficients = 0.095 and -0.017 for bands 3 and 4, respectively), a second trial was developed by modifying the initial variables introduced in the model. Bands 4 and 3 were replaced by the NDVI values, whose mathematic expression, as is well known, includes bands of R and NIR, thereby emphasizing the vegetation cover. In this model, TM band 7 (2.08–2.35 μm) was also incorporated since it did not

Table 7. Summary of Statistics for All Models

Parameters	First Model (Model 1)	Second Model (Model 2)
–2 log likelihood (–2 LL)	457.63	443.23
Nagelkerke r^2	0.65	0.66
Hosmer and Lemeshow: χ^2 (Sig)	12.85 (0.117)	5.47 (0.760)
Percent correct classification (0)	90.2	88.1
Percent correct classification (1)	85.7	79.9
Kappa statistic	0.63	0.65

Table 8. Variables Selected in Model 1

	β^a	Wald Statistic	Significance	Exp(β)
ΔNBR	0.004	20.823	0.000	1.004
TM band 3	0.095	52.158	0.000	1.099
TM band 4	–0.017	10.328	0.001	0.983
Illumination	0.065	27.830	0.000	1.068
Lithology	–1.546	25.581	0.000	0.213
Aspect	3.051	101.622	0.000	21.135
Constant	–7.903	20.765	0.000	0.000

^aEstimated coefficient.

correlate with the NDVI, and the same geophysical variables retained from the first LR trial; results are shown in Table 7. In this case, Nagelkerke r^2 and the Hosmer-Lemeshow test show slightly greater fitting values than those shown in the first trial. ΔNBR, elevation, illumination, NDVI, TM band 7, and the dummy variable aspect were the variables selected in this second trial (model 2) (Table 9). All the β coefficients, except that for NDVI, show positive values. Therefore whereas NDVI exerts a negative impact, increasing the probability of high erosion after fire, the rest of the selected variables are related positively. Nevertheless, only the $\exp(\beta)$ aspect and NDVI values, especially in the latter case, exert great influence on the dependent variable. Differences between the two trials lie not only in the high impact of the NDVI variable when it replaces bands 3 and 4, but also in the elimination of the lithology as an explanatory variable. However, in both cases, the $\exp(\beta)$ coefficients of ΔNBR and illumination only slightly impact probability.

[39] Taking into account the factors and coefficients from both models, predicted probability maps were derived by means of digital processes in ERDAS. Figures 5a and 5b show the probability value of erosion in each cell for the first and second trial, respectively. Outcomes ranged from 0 to 1, with a 0.5 probability value defined as the threshold for distinguishing between the two conditions: high erosion and low erosion after fire.

[40] In the first probability map (derived from the first LR model), areas with the lowest probability of erosion are localized on north facing slopes (with high prefire TM band 4 and low TM band 3 reflectance values) while the areas with the greatest probability correspond to south facing slopes (low TM band 4 values). With reference to the second LR model, areas with the lowest erosion probability are localized similarly on north facing slopes (with high prefire NDVI values) while areas with the greatest probability correspond to sparse vegetation prefire areas located on the south facing slopes. We have observed a high consistency, from a visual point of view, between this second probability map and the NDVI prefire image. Whereas high-probability erosion values are more numerous in the first model, in the second model the low

Table 9. Variables Selected in Model 2

	β^a	Wald Statistic	Significance	Exp(β)
ΔNBR	0.005	28.052	0.000	1.005
Elevation	0.002	8.296	0.004	1.002
Illumination	0.083	32.693	0.000	1.087
Aspect	2.787	87.386	0.000	16.231
NDVI	–7.788	8.199	0.004	0.000
TM band 7	0.035	15.678	0.000	1.036
Constant	–10.678	13.984	0.000	0.000

^aEstimated coefficient.

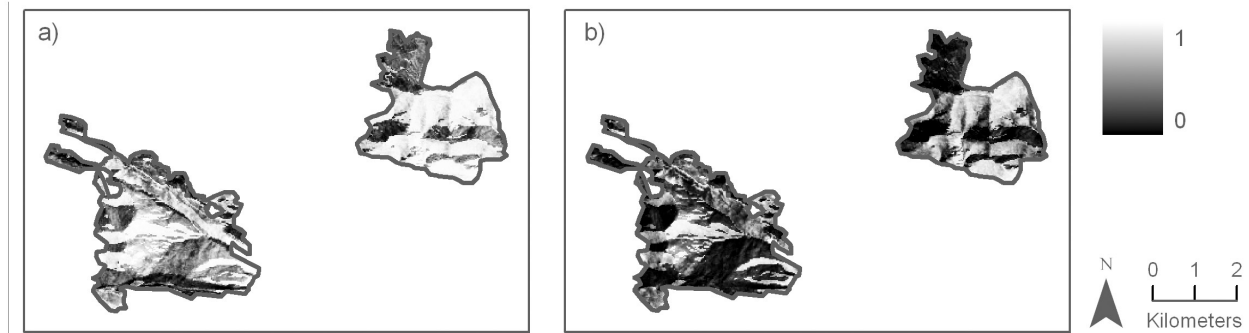


Figure 5. Spatial distribution probability of postfire erosion activity derived from the LR models. Detailed images of the two selected fires. (a) Probability map predicted by model 1. (b) Probability map predicted by model 2.

probability values prove the most important. This fact underscores the sensitivity of the final results in selecting the initial variables. From a statistical point of view, an exponential relationship has been detected between the two models (model 2 = $0.0063e^{4.9023\text{model } 1}$; $r^2 = 0.82$).

[41] Accepting the results of the second model as more closely reflecting reality, the stability and impact of the most important explanatory variables selected by it (NDVI and aspect) were evaluated in a third trial. The potential distorting effects of these models vis-à-vis temporary factors was also verified, with the different meteorological conditions that followed the fires being particularly important. In this third trial, the global sample was divided into two groups, reflecting the dates of the fires ($n = 131$ and $n = 505$ for 1985 and 1986, respectively), with the same explanatory variables observed in the second model similarly considered. The models obtained from the second and sixth steps of both groups were those that features the most consistent values (Hosmer-Lemeshow >0.05) (Table 10). Nagelkerke r^2 values were similar to those obtained for the global sample. NDVI and aspect were the selected variables in both cases (Table 11). Although the impact of aspect variable was similar in the two subsamples, the impact of NDVI proved much more important in the burnt areas of 1986. This fact can be explained by the shady conditions prevalent to most of the areas burnt during this year. On the other hand, ΔNBR , elevation, illumination, and TM band 7 were also selected in the 1986 group.

[42] Finally, to obtain a susceptibility map, a probability map generated with the variables and coefficients from the second model was subdivided into categories. In the literature, several methods can be found, ranging from expert reference studies [Dai and Lee, 2002] to more statistical approaches [Ohlmacher and Davis, 2003]; for further details, see Ayalew and Yamagishi [2005]. In this study, the categorization was made by using regular intervals. Thus the histogram for the probability map was subdivided

Table 10. Overall Model 3 Statistics

Fire Year	Step	Hosmer and Lemeshow		-2 Log Likelihood	Cox and Snell r^2	Nagelkerke r^2
		χ^2	Significance			
1985	2	11.070	0.198	114.766	0.400	0.533
1986	6	11.392	0.180	322.776	0.524	0.700

into five categories of erosion susceptibility: very low, low, medium, high, and very high (Table 12). Sixty percent of the burnt areas registered very low and low susceptibility values. Medium and high-susceptibility areas accounted for 10% and 11% of the areas, respectively, while those areas corresponding to very high susceptibility values constituted 18%; results are shown in Figure 6. The high-susceptibility areas, in white, included those with a probability greater than 80% which corresponded particularly to prefire shrublands and grasslands located on south facing slopes. This fact is especially visible in the fires that occurred in the western quadrant of the study area (Moro, Anzánigo, Triste, and Castillo-Mango). It remains less clear in the fires of the eastern quadrant where the burnt areas, as has been mentioned above, are located on north facing slopes.

5. Discussion

[43] The impact of the NDVI and aspect variables in the LR models shows the role of prefire vegetation and micro-environmental conditions on postfire erosion. The explanatory capacity of both variables is evident if one examines those areas burnt in different years (model 3), or if one adopts a global perspective, taking into account all of the burnt areas addressed in the same analysis (models 1 and 2). In fact, these variables provide evidence of the tolerance levels vis-à-vis environmental degradation processes resulting from the high-severity wildfires. In this sense, tree-plant communities with high NDVI values located on north facing slopes are those most capable of withstanding the negative effects of fire in the medium term. These areas have a greater amount of resources available, and in the

Table 11. Variables Selected in Model 3

Fire Years	Variables	β^a	Wald Statistic	Significance	Exp(3)
1985	aspect	2.971	38.132	0.000	19.503
1985	NDVI	-7.345	8.438	0.004	0.001
1985	constant	2.807	3.915	0.048	16.553
1986	ΔNBR	0.006	19.206	0.000	1.006
1986	elevation	0.003	9.625	0.002	1.003
1986	illumination	0.086	26.845	0.000	1.089
1986	aspect	3.052	63.603	0.000	21.153
1986	NDVI	-9.765	8.352	0.004	0.000
1986	TM band 7	0.034	11.296	0.001	1.034
1986	constant	-10.271	8.615	0.003	0.000

^aEstimated coefficient.

Table 12. Probability Ranges Applied to the Susceptibility Map

Probability Range	Class Name	Coverage, %
<0.20	very low	44.40
0.20–0.40	low	16.13
0.40–0.60	medium	10.01
0.60–0.80	high	11.05
>0.80	very high	18.38

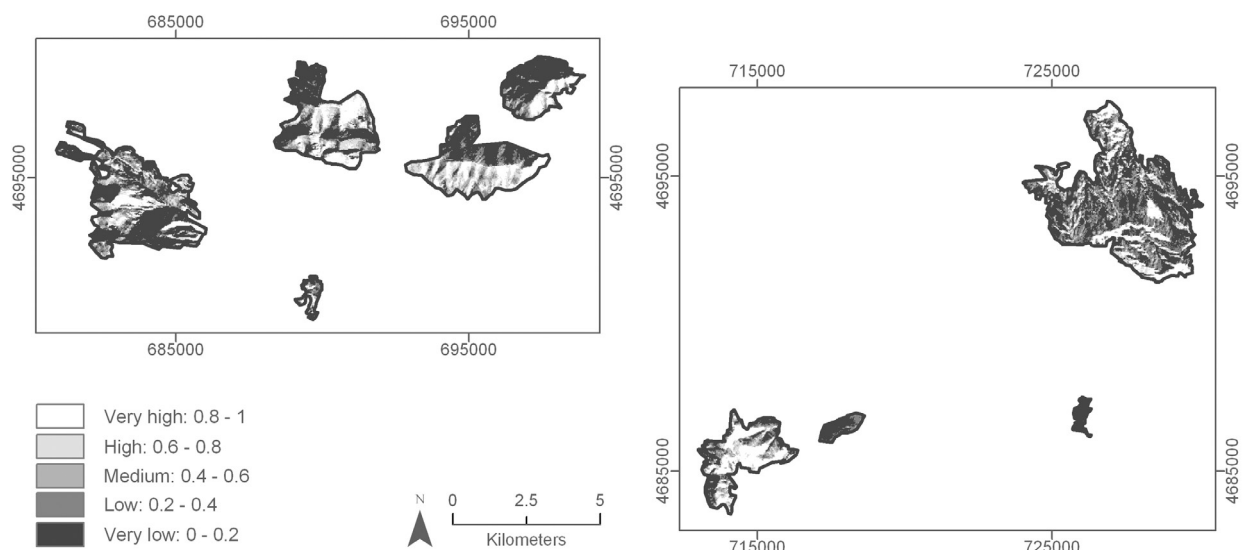
short term, a sufficient recovery level to limit postfire geomorphological reactivation as well. They possess mature biological structures that while needing more time to completely reconstruct themselves, possess a greater inertia since they have not suffered any recent negative disturbances prior to the fire.

[44] General theories associate high severity with the intensification in negative effects (increases in erosion and soil degradation) due to the large biomass present. In fact, in the LR-developed models, the Δ NBR variable has always shown a positive value. Nevertheless, aspect seems to modify the importance of the severity variable, at least in the long term. Environments suffering hydrological shortages, in which the aspect variable influences the soil-vegetation complex, are widely studied, to the extent that the term slope dimorphism has been coined to describe this phenomenon [Bergkamp, 1996; Ibáñez *et al.*, 1997]. The different behaviors exhibited by the opposite slopes can be attributed to the microclimatic variations derived from the distinct radiation that affects slopes. North facing slopes typically experience milder conditions for postfire vegetation recovery; consequently, their edaphogenesis-morphogenesis balance leads to the type of soil formation that allows for greater water-storing capacity, higher infiltration rates, and in short, a clear differentiation in runoff mechanisms. Detailed analysis made by Pérez-Cabello [2002] on burnt areas showed that the interaction between vegetation density and aspect explains in large part postfire erosion.

[45] Other variables, despite having a lower explanatory capacity for erosion distribution, have also been selected by the LR models applied in this work. Some examples are fire severity, lithology, illumination, band 7 TM, elevation, and vegetation structure. Furthermore, in the study area, variables such as climatic indices, vegetation regeneration strategy, or slope were not significant predictors of high erosion, although they can be important in other locations or in analysis geared toward another scale. Special attention must be paid to the slope behavior in the different trials applied. This variable is considered usually one of the factors that most greatly determines the qualitative and quantitative characteristics of runoff generation. However, in the different models developed in this work this variable was never selected. It is necessary to point out that erosion measurements have been made from a long-term perspective; in this respect, slope can have a higher impact on erosion in the short term. Just after the fire, slope is particularly important due to the disappearance of vegetation cover. During this time, slope controls not just the speed of surface and subsurface water flows, but indeed the kinetic energy of the erosive agent, infiltration rates, and sediment conditions. However, the results of the models applied in this study show that, over the long term, other factors replace or neutralize the role played by slope. In any case, one must not forget that LR models are self-explanatory and nonpredictive.

6. Conclusions and Implications

[46] The development of methodologies capable of identifying areas where high erosion could be expected is very useful to support restoration programs in burnt areas. In this respect, the use of nonparametric models (LR) in tandem with environmental information from TM Landsat and DEM, as incorporated into a GIS, can facilitate the management of burnt areas. Taking into account this type of statistical analysis and data, our study shows the great explanatory power of the prefire NDVI and the aspect

**Figure 6.** Susceptibility map of erosion activity following the fire.

variable in generating probability maps regarding postfire erosion in the medium term. High NDVI values in north facing slopes generate a rapid postfire vegetation recovery and reduce the exposure time to erosion agents. By using these two explanatory factors, which have proven the most effective, others of less importance have been identified to explain the dummy variable: fire severity, lithology, illumination, TM band 7, and elevation. In spite of their lower impact, their values in the models are consistent with the studied phenomena. Thus more than 60% of the variations observed in the dependent variable can be explained by the LR model. This percentage decreases to 55% when the global sample is divided by the year the fire occurred.

[47] On the other hand, it is interesting to note that classic risk model predictors (e.g., slope) have not been considered in any of the trials to date. Medium-term estimations of erosion have shown changes in the ranking of explanatory variables. These changes can be explained as stemming from the interactions among these factors over time.

[48] Despite the abovementioned findings, this methodology is capable of identifying erosion-sensitive areas; consequently, it can be used as a planning decision tool in conservation practices following a fire. The consequences of using this kind of cartography in the management of burnt ecosystems are evident. Prior knowledge about which areas have higher probability of developing intense erosion processes allows for better management of burnt restoration programs. Nevertheless, in order to reach a more accurate spatial approach, some aspects must be considered: (1) the need to continue investigating the incorporation of satellite information in predicting erosion processes in burnt areas and the necessity of identifying and mapping fire severity, (2) the introduction of other physical factors related to soil properties such as texture, structure, organic matter content, and depth, and (3) the testing of predictive models that consider erosion as a continuous variable.

[49] **Acknowledgments.** This contribution has been supported financially by the Spanish Ministry of Science and Technology (Ren2002-00133-GLO and CGL2005-04863/CLI) and the Department of Science, Technology and University (Regional Government of Aragón, PIP098/2005).

References

- Aspinall, R. J. (2002), Use of logistic regression for validation of maps of the spatial distribution of vegetation species derived from high spatial resolution hyperspectral remotely sensed data, *Ecol. Modell.*, *157*, 301–312.
- Ayalew, L., and H. Yamagishi (2005), The application of GIS-based logistic regression for landslide susceptibility mapping in the Kakuda-Yahiko Mountains, central Japan, *Geomorphology*, *65*, 15–31.
- Badía, D., C. Martí, E. Reyes, and S. Galindo (1995), Influencia del fuego en la sucesión vegetal de un coscojar en el noreste de España, *Hist. Nat.*, *93*, 83–93.
- Barbosa, P., J. San-Miguel-Ayanz, A. Camia, M. Gimeno, G. Libertà, and G. Schmuck (2004), Assessment of fire damages in the EU Mediterranean countries during the 2003 Forest Fire Campaign, *Rep. SPI.04.64 EN*, Eur. Comm., Brussels.
- Beeson, P. C., S. N. Martens, and D. D. Breshears (2001), Simulating overland flow following wildfire: Mapping vulnerability to landscape disturbance, *Hydrol. Processes*, *15*, 2917–2930.
- Bergkamp, G. (1996), *Mediterranean Ecosystems: Hierarchical Organization and Degradation*, 238 pp., Cip-Gegevens Koninklijke Bibliotheek, The Hague, Netherlands.
- Bertrand, G. (1966), Pour une étude géographique de la végétation, *Rev. Geogr. Pyrenees Sud Ouest*, *37*, 129–144.
- Bobbe, T., H. Lachowski, P. Maus, J. Greer, and C. Dull (2001), A primer on mapping vegetation using remote sensing, *Int. J. Wildland Fire*, *10*, 277–287.
- Bocco, G. (1991), Gully erosion: Processes and models, *Prog. Phys. Geogr.*, *15*, 392–406.
- Braun-Blanquet, J. (1979), *Fitosociología: Bases Para el Estudio de las Comunidades Vegetales*, 820 pp., H. Blume, Madrid.
- Cannon, S. H., E. R. Bigio, and E. Mine (2001), A process for fire-related debris flow initiation, Cerro Grande fire, New Mexico, *Hydrol. Processes*, *15*, 3011–3023.
- Cerdà, A. (1998), Changes in overland flow and infiltration after a range-land fire in a Mediterranean scrubland, *Hydrol. Processes*, *12*, 1031–1042.
- Cerdà, A., and S. H. Doerr (2005), Influence of vegetation recovery on soil hydrology and erodibility following fire: An 11-year investigation, *Int. J. Wildland Fire*, *14*, 423–437.
- Chavez, P. S. (1996), Image-based atmospheric corrections: Revisited and improved, *Photogramm. Eng. Remote Sens.*, *62*(9), 1025–1036.
- Chuvieco, E., F. J. Salas, J. R. de la Riva, F. Pérez-Cabello, and N. Lana-Renault (2004), Métodos para la integración de variables de riesgo: El papel de los sistemas de información geográfica (SIG), in *Nuevas tecnologías para la estimación del riesgo de incendios forestales*, edited by E. Chuvieco, pp. 143–183, Inst. de Econ. y Geogr., Cons. Super. de Invest. Cient., Madrid.
- Collins, J. B., and C. E. Woodcock (1996), An assessment of several linear change detection techniques for mapping forest mortality using multi-temporal Landsat TM data, *Remote Sens. Environ.*, *56*, 66–77.
- Conese, C., G. Maracchi, F. Miglietta, F. Maselli, and V. M. Sacco (1988), Forest classification by principal components analysis of TM data, *Int. J. Remote Sens.*, *9*(10–11), 1597–1612.
- Congalton, R. G., and K. Green (1999), *Assessing the Accuracy of Remotely Sensed Data: Principles and Practices*, 137 pp., Lewis, Boca Raton, Fla.
- Crist, E. P., and R. C. Cicone (1984), A physically-based transformation of Thematic Mapper data—The TM tasseled cap, *IEEE Trans. Geosci. Remote Sens.*, *22*(3), 256–263.
- Dai, F. C., and C. F. Lee (2002), Landslide characteristics and slope instability modeling using GIS, Lantau Island, Hong Kong, *Geomorphology*, *42*, 213–228.
- DeBano, L. F., D. G. Neary, and P. F. Ffolliott (1998), *Fire's Effects on Ecosystems*, 333 pp., John Wiley, Hoboken, N. J.
- de Jong, S. M., M. L. Paracchini, F. Bertolo, S. Folving, J. Megier, and A. P. J. de Roo (1999), Regional assessment of soil erosion using the distributed model SEMMED and remotely sensed data, *Catena*, *37*, 291–308.
- Díaz-Delgado, R., and X. Pons (2001), Spatial patterns of forest fires in Catalonia (NE of Spain) along the period 1975–1995: Analysis of vegetation recovery after fire, *For. Ecol. Manage.*, *147*, 67–74.
- Díaz-Delgado, R., F. Lloret, and X. Pons (2003), Influence of fire severity on plant regeneration by means of remote sensing imagery, *Int. J. Remote Sens.*, *24*(8), 1751–1763.
- Díaz-Fierros, F., E. Benito, J. A. Vega, A. Castelao, B. Soto, R. Pérez, and T. Taboada (1990), Solute loss and soil erosion in burnt soil from Galicia NW Spain, in *Fire in Ecosystem Dynamics*, edited by J. G. Goldammer and M. J. Jenkins, pp. 103–116, SPB Acad., The Hague, Netherlands.
- Dieckmann, H., H. Motzer, H. P. Harres, and O. Seuffert (1992), Vegetation and erosion: Investigations on erosion plots in southern Sardinia, *Geokoplos*, *3*, 139–149.
- Epting, J., D. Verbyla, and B. Sorbel (2005), Evaluation of remotely sensed indices for assessing burn severity in interior Alaska using Landsat TM and ETM+, *Remote Sens. Environ.*, *96*, 328–339.
- Escuin, S., P. Fernández-Rebollo, and R. M. Navarro (2002), Aplicación de escenas Landsat a la asignación de grados de afectación producidos por incendios forestales, *Rev. Teledetección*, *1*, 25–36.
- Fernández, S., J. Marquinez, and R. Menéndez-Duarte (2005), A susceptibility model for post wildfire soil erosion in a temperate oceanic mountain area of Spain, *Catena*, *61*(2–3), 256–272.
- Food and Agricultural Organization (FAO) (1977), *Guía para la descripción de perfiles de suelo*, 2nd ed., 70 pp., Rome.
- Food and Agricultural Organization (FAO) (1980), *Metodología provisional para la evaluación de la degradación de suelos*, 86 pp., Rome.
- Fraser, R. H., T. A. Abuelgasim, and R. Latifovic (2005), A method for detecting large-scale forest cover change using coarse spatial resolution imagery, *Remote Sens. Environ.*, *95*, 414–427.
- Fung, L., and E. LeDrew (1987), Application of principal components analysis to change detection, *Photogramm. Eng. Remote Sens.*, *53*, 1649–1658.
- Gorsevski, P. V., P. Gessler, and R. B. Foltz (2000), Spatial prediction of landslide hazard using logistic regression and GIS, in *4th International Conference on Integrating GIS and Environmental Modeling, Proceedings [CD-ROM]*, Paper 305, 9 pp., Coop. Inst. for Res. in the Environ. Sci., Boulder, Colo.
- Hanes, T. J. (1971), Succession after fire in the chaparral of southern California, *Ecol. Monogr.*, *41*, 27–52.

- Helvey, J. D. (1980), Effects of a north central Washington wildfire on runoff and sediment production, *Water Resour. Bull.*, 16(4), 31–49.
- Ibáñez, J. J., B. L. Valero, and C. Machado (Eds.) (1997), *El paisaje mediterráneo a través del espacio y del tiempo. Implicaciones en la desertificación*, 477 pp., Geoforma Ed., Logroño, Spain.
- Jakubauskas, M., K. P. Lulla, and P. W. Mausel (1990), Assessment of vegetation change in a fire-altered forest landscape, *Photogramm. Eng. Remote Sens.*, 56, 371–377.
- Kasischke, E. S., and N. H. F. French (1995), Locating and estimating the areal extent of wildfires in Alaskan boreal forests using multiple-season AVHRR NDVI composite data, *Remote Sens. Environ.*, 51, 263–275.
- Keeley, J. E. (1986), Resilience of Mediterranean shrub communities to fires, in *Resilience in Mediterranean-Type Ecosystems*, edited by B. Dell, A. J. M. Hopkins, and B. B. Lamont, pp. 95–112, Springer, New York.
- Key, C. H., and N. C. Benson (2006), Landscape assessment (LA)-sampling and analysis methods, *Gen. Tech. Rep. RMRS-GTR-164-CD*, 51 pp., Rocky Mtn. Res. Stn., For. Serv., U.S. Dep. of Agric., Ogden, Utah.
- King, C., V. Lecomte, Y. Le Bissonnais, N. Baghdadi, V. Souchère, and O. Cerdan (2005), Remote-sensing data as an alternative input for the “STREAM” runoff model, *Catena*, 62, 125–135.
- Martínez-Casasnovas, J. A., and R. M. Poch (1998), Estado de conservación de los suelos de la cuenca del embalse Joaquín Costa, *Limnetica*, 14, 83–91.
- Mataix-Solera, J., and S. H. Doerr (2003), Hydrophobicity and aggregate stability in calcareous topsoils from fire-affected pine forests in south-eastern Spain, *Geoderma*, 118, 77–88.
- May, T. (1991), Observaciones y reflexiones sobre el comportamiento tras fuego de algunas especies de la zona mediterránea de Andalucía, *Oriental, Ecología*, 5, 125–134.
- McNabb, D. H., and F. J. Swanson (1990), Effects of fire on soil erosion, in *Natural and Prescribed Fire in the Pacific Northwest Forests*, edited by J. D. Walsad, S. R. Radosevich, and D. V. Sandberg, pp. 159–176, Oregon State Univ. Press, Corvallis.
- Menard, S. (1995), *Applied Logistic Regression Analysis, Ser. Quant. Appl. Soc. Sci.*, vol. 106, Sage, Thousand Oaks, Calif.
- Meyer, G. A., and S. G. Wells (1997), Fire-related sedimentation events on alluvial fans, Yellowstone National Park, USA, *J. Sediment. Res.*, 67, 776–791.
- Meyer, G. A., J. L. Pierce, S. H. Wood, and A. J. T. Jull (2001), Fire, storms, and erosional events in the Idaho batholith, *Hydrol. Processes*, 15, 3025–3038.
- Miller, J. D., and S. R. Yool (2002), Mapping forest post-fire canopy consumption in several overstory types using multi-temporal Landsat TM and ETM data, *Remote Sens. Environ.*, 82, 481–496.
- Minnich, R. A. (1983), Fire mosaics in southern California and northern Baja California, *Science*, 219, 1287–1294.
- Moody, J. A., and D. A. Martin (2001), Post-fire, rainfall intensity-peak discharge relations for three mountainous watersheds in the western USA, *Hydrol. Processes*, 15, 2981–2993.
- Naveh, Z. (1974), Effects of fire in the Mediterranean region, in *Fire and Ecosystems*, edited by T. T. Kozlowski and C. E. Ahlgreen, pp. 372–390, Elsevier, New York.
- Naveh, Z. (1990), Fire in the Mediterranean—A landscape ecological perspective, in *Fire in Ecosystems Dynamics*, edited by J. G. Goldammer and M. J. Jenkins, pp. 1–20, SPB Acad., The Hague, Netherlands.
- Neary, D. G., C. C. Klopatek, F. F. DeBano, and P. F. Follitt (1999), Fire effects on belowground sustainability: A review and synthesis, *For. Ecol. Manage.*, 122, 51–71.
- Ohlmacher, G. C., and J. D. Davis (2003), Using multiple logistic regression and GIS technology to predict landslide hazard in northeast Kansas, USA, *Eng. Geol.*, 69, 331–343.
- Papió, C. (1988), Respuesta al fuego de las principales especies de la vegetación de Garraf (Barcelona), *Orsis*, 3, 87–103.
- Patterson, M. W., and S. R. Yool (1998), Mapping fire-induced vegetation mortality using Landsat Thematic Mapper data: A comparison of linear transformation techniques, *Remote Sens. Environ.*, 65, 132–142.
- Pérez-Cabello, F. (2002), *Paisajes forestales y fuego en el Prepirineo occidental oscense: Un modelo regional de reconstrucción ambiental, Ser. Invest.*, vol. 33, Publ. del Cons. Prot. de la Nat. de Aragón, Zaragoza, Spain.
- Pérez-Cabello, F., and J. R. de la Riva (1998), El empleo de imágenes Landsat TM para la detección y cartografía de áreas incendiadas en el Prepirineo occidental oscense, *Geographica*, 36, 131–145.
- Pons, X., and L. Solé-Sugrañes (1994), A simple radiometric correction model to improve automatic mapping of vegetation from multispectral satellite data, *Remote Sens. Environ.*, 48, 191–204.
- Rivas-Martínez, S. (1987), Memoria del mapa de las series de vegetación, report, Minist. de Agric., Pesca y Alimentación, Madrid.
- Rivas-Martínez, S., and J. Loidi (1999), Bioclimatology of the Iberian Peninsula, *Itinera Geobot.*, 13, 41–47.
- Robichaud, P. R., and R. E. Brown (1999), What happened after the smoke cleared: Onsite erosion rates after a wildfire in eastern Oregon, in *Proceedings of the Annual Summer Specialty Conference*, vol. 2, *Wildland Hydrology*, pp. 419–426, Am. Water Resour. Assoc., Middleburg, VA.
- Robichaud, P. R., and T. A. Waldrop (1994), A comparison of surface runoff and sediment yields from low-and-high severity site preparation burns, *Water Resour. Bull.*, 30, 27–34.
- Rogan, J., and J. Franklin (2001), Mapping wildfire burn severity in southern California forests and shrublands using enhanced Thematic Mapper imagery, *Geocarto Int.*, 16(4), 89–99.
- Ruiz de la Torre, J. (1992), Mapa Forestal de Aragón: Huesca (hoja 8-3), Minist. de Agric., Pesca y Alimentación, Madrid.
- Ruiz-Gallardo, J. R., S. Castaño, and A. Calera (2004), Application of remote sensing and GIS to locate priority intervention areas after wildland fires in Mediterranean systems: A case study from south-eastern Spain, *Int. J. Wildland Fire*, 13, 241–252.
- Siegert, F., and A. Hoffmann (2000), The 1998 forest fires in east Kalimantan (Indonesia): A quantitative evaluation using high resolution, multi-temporal ERS-2 SAR images and NOAA-AVHRR hotspot data, *Remote Sens. Environ.*, 72, 64–77.
- Soler, M., and M. Sala (1992), Effects of fire and of clearing in a Mediterranean *Quercus ilex* woodland: An experimental approach, *Catena*, 19, 321–332.
- Soto, B., E. Benito, R. Basanta, and F. Díaz-Fierros (1991), Influence of antecedent soil moisture on pedological effects of fire, in *Soil Erosion and Degradation as a Consequence of Forest Fires*, edited by M. Sala and J. L. Rubio, Geoforma Ed., Logroño, Spain.
- Tárrega, R., and E. Luis-Calabuig (1987), Effects of fire on structure, dynamics and regeneration of *Quercus pyrenaica* ecosystems, *Ecol. Mediter.*, 13(4), 79–86.
- Tárrega, R., and E. Luis-Calabuig (1989), Análisis temporal durante tres años consecutivos de las primeras fases de regeneración post-fuego en robledales de la provincia de León, *Stud. Ecol.*, 6, 205–216.
- Townshend, J. R. G., and C. O. Justice (1986), Analysis of the dynamics of the African vegetation using the normalized difference vegetation index, *Int. J. Remote Sens.*, 7, 1435–1445.
- Trabaud, L. (1990), Fire resistance of *Quercus coccifera* L. Garrigue, in *Proceedings of the Third International Symposium on Fire Ecology*, edited by J. G. Goldammer and M. J. Jenkins, pp. 21–32, SPB Acad., The Hague, Netherlands.
- Trabaud, L. (2002), Post-fire vegetation recovery and dynamics in the Mediterranean area, in *Fire, Landscape and Biodiversity: An Appraisal of the Effects and Effectiveness*, edited by G. Pardini and J. Pintó, pp. 39–56, Inst. de Medi Ambient, Univ. de Girona, Girona, Spain.
- Trabaud, L., and J. Valina (1998), Importance of tree size in *Pinus halepensis* fire survival, in *Fire Management and Landscape Ecology*, edited by L. Trabaud, pp. 189–196, Int. Assoc. of Wildland Fire, Hot Springs, S. D.
- Tucker, C. J., C. L. Vanpreat, M. J. Sharman, and G. Van Ittersum (1985), Satellite remote sensing of total herbaceous biomass production in the Senegalese Sahel: 1980–1984, *Int. J. Remote Sens.*, 7, 233–249.
- Vallejo, V. R., and J. A. Alloza (1998), The restoration of burned lands: The case of eastern Spain, in *Large Forest Fires*, edited by J. M. Moreno, pp. 91–108, Backhuys, Leiden, Netherlands.
- Van Wageningen, J. W., R. R. Root, and C. H. Key (2004), Comparison of AVIRIS and Landsat ETM+ detection capabilities for burn severity, *Remote Sens. Environ.*, 92, 397–408.
- Vera de La Fuente, M. L. (1994), Regeneración de un aulagar con *Ulex europaeus* después de un incendio en el norte de España, *Pirineos*, 143–144, 87–98.
- Viedma, O., J. Meliá, D. Segarra, and J. García-Haro (1997), Modelling rates of ecosystem recovery after fires by using Landsat TM data, *Remote Sens. Environ.*, 61, 383–398.
- Wilson, C. J., J. W. Carey, P. C. Beeson, M. O. Gard, and L. J. Lane (2001), A GIS-based hillslope erosion and sediment delivery model and its application in the Cerro Grande burn area, *Hydrol. Processes*, 15, 2995–3010.
- Wondzell, S. M., and J. G. King (2003), Postfire erosional processes in the Pacific Northwest and Rocky Mountain regions, *For. Ecol. Manage.*, 178, 75–87.

J. de la Riva Fernández, A. García-Martín, R. Montorio Llovería, and F. Pérez-Cabello, Department of Geography and Spatial Management, University of Zaragoza, E-50009 Zaragoza, Spain. (delariva@unizar.es; algarcia@unizar.es; montorio@unizar.es; fcabello@unizar.es)